The relationship between fine structure and physicochemical properties of starches from wheat (*Triticum aestivum* L.) varieties

Saddam Mustafa[1], Haiam O. Elkatry[2], Mohamed El Oirdi[3], Chengyi Sun[1], Zhijie Zhu[1], Hossam S. El-Beltagi[4], Abdelrahman R. Ahmed[2*], Xianfeng Du[1*]

[1]Key Laboratory of Jianghuai Agricultural Product Fine Processing and Resource Utilization, Ministry of Agriculture and Rural Affairs, Anhui Engineering Research Center for High-Value Utilization of Characteristic Agricultural Products, College of Tea & Food Science and Technology, Anhui Agricultural University, Hefei, P.R. China; [2]Food and Nutrition Science Department, Agricultural Science and Food, King Faisal University, Al-Ahsa, Saudi Arabia; [3]Department of Life Sciences, College of Science, King Faisal University, Al Ahsa 31982, Saudi Arabia; [4]Agricultural Biotechnology Department, College of Agriculture and Food Sciences, King Faisal University, Al-Ahsa, Saudi Arabia

***Corresponding Authors:** Xianfeng Du, Key Laboratory of Jianghuai Agricultural Product Fine Processing and Resource Utilization, Anhui Engineering Research Center for High-Value Utilization of Characteristic Agricultural Products, College of Tea & Food Science and Technology, Anhui Agricultural University, Hefei 230036, P.R. China. Email: dxf@ahau.edu.cn; Abdelrahman R. Ahmed, Food and Nutrition Science Department, Agricultural Science and Food, King Faisal University, Al-Ahsa 31982, Saudi Arabia. Email: arahmed@kfu.edu.sa

Academic Editor: Prof. Alessandra Del Caro–(SISTAL)—University of Sassari, Italy

Received: 29 October 2024; Accepted: 27 January 2025; Published: 1 April 2025

ORIGINAL ARTICLE

Abstract

Considering the impact of geographic location on starch properties, this research investigates the relationship between fine structure and physicochemical properties of starch isolated from three wheat varieties (Pw1, Sw2, and Hw3) cultivated in Pakistan. The starch granules displayed a range of morphologies, including large lenticular and irregularly disk-like forms as well as smaller oval shapes. Among the starches, Sw2 exhibited the lowest amylose content, while Pw1 showed the longest average amylopectin chain length and the highest molecular weight. X-ray diffractometer and ^{13}C solid-state nuclear magnetic resonance analyses revealed typical A-type diffraction patterns in all three starches, with Pw1 having the highest relative crystallinity. FT-IR results indicated that Pw1 possessed the most ordered structure, as reflected by the highest R_{1047}–R_{1022} ratio. Findings of differential scanning calorimetry showed that Pw1 had an elevated gelatinization temperature, resulting from its high proportion of long amylopectin chains (degree of polymerization [DP] > 37). In contrast, Hw3 displayed the highest peak and setback viscosities because of its substantial proportion of amylopectin short chains. Hw3 also demonstrated the highest water solubility and swelling power because of its high amylose content. All starches exhibited shear-thinning behavior, with Sw2 having the lowest storage modulus in frequency sweep tests. Additionally, Sw2 showed the greatest oil- and water-absorption capacities, which is associated with its low amylose content. Variations in the fine structure of starch account for the distinct physicochemical properties observed among the wheat varieties, playing an essential role in the tailored selection of wheat products based on their characteristics.

Keywords: multi-scale structure; physicochemical properties; relationship; wheat starch

Introduction

Wheat (*Triticum aestivum* L.) is a globally cultivated, consumed, and traded grain, encompassing a vast diversity of varieties. In all, 43 countries regularly consume wheat-based foods, representing 35% of the global population. In recent years, Pakistan has been one of the leading global producers of wheat (Mitura *et al.*, 2023). For centuries, wheat has been a staple in the local diet, providing essential nutrients for health (Kumar and Khatkar, 2017). Wheat is predominantly used for food (67%), with significant proportions dedicated to feed (20%), seed (7%), and industrial applications (6%) (Maningat *et al.*, 2009). Starch, which constitutes approximately 70–75% of wheat grains, is primarily located in the endosperm and comprises amylopectin and amylose. The proportions of amylose and amylopectin vary across different wheat varieties (Shevkani *et al.*, 2017). Starch is a vital carbohydrate integral to human dietary intake and has extensive applications in non-food industries (Xia *et al.*, 2016). Starches derived from various plant origins, including those from identical species cultivated in diverse conditions, display distinct structural compositions, functional characteristics, and applications (Dos Santos *et al.*, 2016). The physicochemical and functional properties of wheat starches are not homogeneous; they vary depending on the wheat variety, regional growing conditions, and harvest time (Huang *et al.*, 2022). Extensive research has been conducted into the structural and physicochemical features of wheat starches grown in various geographical regions (Hung *et al.*, 2007; Karwasra *et al.*, 2017; Shevkani *et al.*, 2011; Zhang *et al.*, 2013b; Zhao *et al.*, 2019; Wickramasinghe *et al.*, 2005). Substantial differences in the physicochemical characteristics of starch have been documented among various wheat varieties. Research conducted by Debon and Tester (2000) and Tester and Karkalas (2001) has shown that environmental factors have a more pronounced impact on starch characteristics relative to differences among varieties. This suggests that the morphological and physicochemical characteristics previously established for starches from wheat varieties cultivated in other regions may not be directly applicable to those grown in Pakistan. Moreover, there is a notable lack of information regarding the structural and physicochemical characteristics of starch extracted from Pakistani wheat varieties. Therefore, the fine structure and physicochemical characteristics of starches extracted from Pakistani wheat varieties, currently utilized in the food industry, were investigated. This information would provide significant insights into their use within the food industry and other sectors.

Material and Method

The commercially mature seeds of three wheat varieties (Punjab wheat (Pw1), Sindh wheat (Sw2), and Haronabad wheat (Hw3)) were obtained from a seed supplier in Pakistan. Amylopectin standards, along with amyloglucosidase (A7095, enzyme activity ≥ 300 U/mL), porcine pancreatic α-amylase (PPA, A3176, EC3.2.1.1, type VI-B, activity: 16 U/mg), isoamylase (EC3.2.1.68, from Pseudomonas sp., enzyme activity ≥ 1,000 U/μL), and pullulanase (EC3.2.1.41, from Klebsiella planticola, enzyme activity ≥ 106 U/mg) were provided by Sigma-Aldrich (St. Louis, MO, USA). All other reagents utilized were of analytical quality.

Starch isolation

For starch extraction, we employed the technique outlined by Singh *et al.* (2004). Initially, wheat seeds underwent overnight immersion in an excess of deionized water at 20°C; after that, the seeds were pulverized in a laboratory blender, and the resulting flour was suspended in NaOH 0.3% at 25°C for 18 h. In the following step, the starch slurry underwent filtration through nylon cloth with a mesh size of 100 μm. Following this, centrifugation at 3,000 rpm for 15 min (repeated for three times) was employed to remove both supernatant and upper gray layer. Later, the residual white sediments were subjected to triple washing with distilled water until they reached a neutral pH and the resulting precipitates were subjected to drying at 40°C for 12 h. After being crushed, the wheat starches were put through an 80-mesh filter and sealed in bags.

Chemical composition

Wheat seeds were crunched into flour and sifted through a 100-micron mesh. The resulting flour was subsequently used to assess the overall protein and starch contents. The total starch content in the wheat flour was determined using the Megazyme Total Starch assay kit. The ash, lipid, protein, and moisture contents were determined following the procedure described by Wang *et al.* (2015). The amylose content was examined following the methodology described by Li *et al.* (2015).

Morphology of starch granules

Scanning electron microscope (SEM) analysis

The surface morphology of starch granules was examined at 1,000× magnification using a scanning electron microscope (SEM S-4800, Hitachi, Japan) with an acceleration voltage of 3 kV. Starch samples were attached to circular aluminum stubs using an adhesive tape and vacuum, followed by a thin gold coating.

Confocal laser scanning microscopy

The morphological characteristics of the samples were examined with an Olympus FV10 confocal laser scanning

microscope (CLSM) in fluorescent mode with an excitation wavelength of 488 nm by following the procedure outlined by Zhou *et al.* (2015). A fluorescein 5-isothiocyanate (FITC) solution (2 mg/mL, 40 µL) was mixed with a starch suspension (100 µL, prepared by dissolving 10.00 mg of starch in distilled water to achieve a concentration of 0.10 mg/mL) and kept in the dark for 60 min. After staining, 2 µL of the suspension was extracted and dispersed in a glycerol-water mixture (1:1, mass ratio) on a microscopic slide. The samples were initially analyzed using fluorescence and polarized light, followed by an observation under standard light microscopy.

Starch particle size distribution

A Master-Sizer 2000 (Malvern Instruments Ltd., UK) was utilized to assess the particle size distribution of wheat starches by following an earlier method with slight modifications (de Souza Fernandes *et al.*, 2019). Starch samples were mixed and agitated at 2,000 rpm while being diluted in distilled water. Sufficient starch was dispersed to achieve an optimal obscuration factor of 10–12%. The results were generated and visualized using the instrument's integrated software.

Molecular weight and chain length distribution

The amylopectin chain length distribution and molecular weight of the starches were analyzed using a method described previously (Deng *et al.*, 2023). The distribution of chain lengths was analyzed using high-performance anion exchange chromatography coupled with pulsed amperometric detection (HPAEC-PAD) on a Dionex ICS-5000 system (Dionex Corp, Sunnyvale, CA, USA). The sample (100 µL) was injected into the system, and elution was performed at a flow rate of 1 mL/min using two eluents: eluent A (150-mM sodium hydroxide) and eluent B (150-mM sodium hydroxide with 500-mM sodium acetate). The elution gradient was as follows: 0–9 min, 15–36% B; 9–18 min, 36–45% B; 18–110 min, 45–100% B; 100–112 min, 100–15% B; 112–130 min, 15% B. The system was equilibrated with 15% eluent B for 60 min to stabilize (Li *et al.*, 2020). The molecular weight of the starches was assessed using gel permeation chromatography (GPC) combined with multi-angle laser light scattering (MALLS) and refractive index detection (RI) on a U3000 system (Thermo, USA).

Structure characterization

X-ray diffraction analysis

The crystalline structure of wheat starches was examined with an X-ray diffractometer (XRD; X'Pert PRO, Tokyo, Japan). The diffraction patterns were captured at a scan rate of 5°/min, with operating conditions set at 40 kV and 40 mA. Data were acquired over a 2θ (2 theta) range from 5° to 50°. The experimental data were analyzed with MDI Jade 6 software, which calculated crystallinity by integrating the areas corresponding to the crystalline and amorphous regions.

^{13}C CP/MAS solid-state nuclear magnetic resonance (NMR) spectroscopy analysis

The molecular configuration of starches was analyzed using a solid-state ^{13}C NMR spectrometer (AVANCE III HD NMR, Bruker Ltd., Switzerland) fitted with a 4-mm H/X resonance magic angle spinning (MAS) solid broadband probe. The data were collected with a spectral width of 50 kHz, at an acquisition duration of 0.02 s, a resonance frequency of 100.6 MHz, and 2,048 scans. Chemical shifts (δ) were expressed in parts per million (ppm). The NMR data were analyzed with the MestReNova software, version 6.1 (Mestrelab Research, Switzerland AG).

Fourier transform infrared spectroscopy (FT-IR)

An FT-IR spectrometer (Nicolet 6700, Thermo Fisher, IL, USA) was utilized to examine the short-range molecular structure of wheat starches. The starch samples were mixed with dry KBr powder in a 1:100 (w/w) ratio, and the mixture was compressed into pellets. The spectrum was recorded in the range of 400–4,000 cm^{-1} with a resolution of 4 cm^{-1}. The absorbance ratio between 1,047 cm^{-1} and 1022 cm^{-1} was identified using the Omnic software (Version 8.2, Thermo Fisher).

Physicochemical properties

Pasting properties

A rapid viscosity analyzer (RVA; TecMaster, Perten, Australia) evaluated the pasting characteristics of the starch samples, utilizing the procedure outlined by Gunaratne *et al.* (2018). In this procedure, 3 g of starch was blended with 25 mL of distilled water and agitated at 960 rpm for 10 s. The mixture was kept at 50°C for 1 min, and then gradually heated at a rate of 5°C/min until it reached 95°C, where it was maintained for 2.5 minutes. Subsequently, it was cooled down to 50°C at a rate of 6°C/min and held at this temperature for an additional 1.5 min. The RVA curve was used to evaluate various parameters, such as pasting temperature, peak, setback, and breakdown viscosity.

Rheological properties

Frequency scans were performed within the linear viscoelastic range (at 10% strain) to evaluate the sample's rheological properties. The tests were conducted at a steady temperature of 25°C, over a frequency span of 0.1–100 rad/s, measuring viscous modulus (G") and elastic modulus (G'). A rotating rheometer (DHR-1, TA Instruments, USA) was used to assess rheological features of the samples. A sufficient quantity of starch was

dissolved in distilled water to make a 5% solution, which was then boiled for 30 min to ensure complete gelatinization before cooling to 25°C. Under oscillatory conditions, a plate with a 40-mm diameter and a 1-mm gap was used to identify the linear viscoelastic region of the starch. The experimental setup was adapted from the technique outlined by Li *et al.* (2017). During flow scanning rheological measurements, the temperature was kept constant at 25°C, and the shear rate ranged from 0 to 100 s^{-1}. The experimental data were applied to the power-law equation, with an empty crucible serving as a reference control:

$$\tau = K\gamma^{n},$$

where shear stress is denoted by τ (Pa), shear rate by γ (s^{-1}), consistency coefficient by K (Pa s^{n}), and flow behavior index by n.

Thermal properties

Thermal properties of the starch samples were examined using a DSC 8000 instrument (Perkin Elmer Corporation, USA) according to the procedure outlined by Zhang *et al.* (2020). Precisely, 2 mg of starch powder was placed in a crucible and mixed with 6 μL of distilled water. The containers were sealed, shaken thoroughly, and stored at room temperature for 12 h. The samples were heated in a nitrogen environment at a flow rate of 20 mL/min, starting from 30°C and increasing to 110°C, at a rate of 10°C/min.

Swelling power and water solubility

The swelling power and solubility of wheat starches were assessed using the procedure outlined by Wongsagonsup *et al.* (2014). A suspension of starch (0.5 g) was prepared in 15 mL of distilled water and maintained in a shaking water bath set to 85°C for 30 min. The suspension was allowed to cool to room temperature (25°C) and centrifuged at 2,200× *g* for 15 min to isolate swollen paste sediment from supernatant. The solubilized starch content was measured by drying the supernatant at 110°C overnight. The weight of the solubilized starch in the supernatant and the swollen starch sediment was recorded and subsequently used to calculate the swelling power and solubility of the starch as outlined below:

$$\text{Swelling power (g/g)} = \frac{\text{Wet weight of swollen starch sediments}}{\text{Dry weight of starch} \times (100 - \%\text{solubility})},$$

$$\text{Solubility (\%)} = \frac{\text{Dry weight of solubilized starch}}{\text{Dry weight of starch}} \times 100.$$

Absorption of water and oil

A starch sample (100 mg) was transferred to a 1-mL centrifuge tube, followed by the addition of 1 mL of soybean oil or distilled water. The blend was vigorously agitated for 20 min and then centrifuged at 4,000 rpm for 15 min. The supernatant was decanted, and any residual water or oil was removed with filter paper. Once no further liquid was visible on the filter paper, the sample was weighed. The absorption capacity (g/g) was determined by dividing the weight of the wet precipitate by the dry weight of the sample (Song *et al.*, 2020).

Statistical analysis

The results, expressed as mean values ± standard deviation, are derived from three repetitions of the experiments. Statistical analyses were conducted using the IBM SPSS 19.0 software. Duncan's test, with a significance level of $p < 0.05$, was used to detect differences between mean values. Statistical significance was established at $p < 0.05$. Additionally, the Pearson correlation coefficient was computed to assess relationships between variables.

Result and Discussion

Chemical composition of wheat flour

The chemical composition of three types of whole wheat flour is shown in Table 1. The moisture content of sample starches ranged from 7.94% to 10%. Protein content varied between 8.56% and 12.41%, with Sw2 exhibiting significantly higher levels ($p \leq 0.05$). The protein levels reported in this study was within the range as documented in the literature for other wheat varieties (Liu *et al.*, 2015). The fat content ranged from 3.71% to 5.47%, with Hw3 having the highest value. The ash content also exhibited negligible variation ($p > 0.05$), ranging from 2.57% to 2.68%, slightly higher than the previously reported values for whole wheat flour (Bashir *et al.*, 2017; Liu *et al.*, 2015). Among the varieties, Hw3 had the highest total starch content (61.83%) whereas Sw2 had the lowest starch content value (47.8%). The starch content in this study was somewhat lower than those reported for other wheat varieties in prior studies (Labuschagne *et al.*, 2007; Li *et al.*, 2016a; Seib *et al.*, 1997). Amylose content varied significantly ($p < 0.05$) across wheat starches, ranging from 36.03% in Sw2 to 37.74% in Pw1 and 38.44% in Hw3 (Table 1), which were higher than previously reported values (Cai and Shi, 2010). Variations in amylose and amylopectin contents among different starch varieties have been attributed to enzymatic processes responsible for synthesizing branched and linear α-glucans within starch particles (Li *et al.*, 2014).

Table 1. Chemical composition of starch varieties.

Samples	Chemical composition					
	Ash content (%)	Protein content (%)	Fat content (%)	Moisture (%)	Total starch (%)	Amylose (%)
PW1	2.68±0.62^{b}	8.56±0.94^{b}	3.71±0.87^{c}	10.08±0.21^{a}	53.72 ±0.22^{b}	37.74 ±0.35^{b}
SW2	2.83 ±0.57^{a}	12.41±0.21^{a}	4.06±0.39^{b}	7.94±0.37^{c}	47.83±0.27^{c}	36.03±0.34^{c}
HW3	2.57±0.43^{c}	8.89±1.62^{b}	5.47±0.46^{a}	9.12±0.13^{b}	61.83±0.25^{a}	38.44±0.36^{a}

Values are means ± standard deviation (n = 3). Different superscripted letters within a column intend significant differences ($p < 0.05$).

Morphological features of starch

The micrographs of wheat starches were obtained using polarized light microscopy (PLM), light microscopy (LM), SEM, and CLSM (Figure 1). The SEM analysis revealed significant variations in the size and shape of starch particles among the three starches. Wheat starch consisted of two distinct types of particles: A-type particles, which were lenticularly large and irregularly disc-shaped, and B-type particles, which were elliptical, small, and oval (Figure 1). Pw1 and Sw2 starches displayed a higher quantity of A-type particles, with only a few B-type particles. On the other hand, Hw3 starch had a considerable number of B-type particles. The surface of most starch granules appeared smooth, although some larger granules exhibited visible grooves or indentations, consistent with previous studies (Salman *et al.*, 2009; Wang *et al.*, 2014; Zhang *et al.*, 2013b). The indentations or grooves on large particles were probably formed by the impressions of protein bodies or small particles during the process of grain development (Shevkani *et al.*, 2017). To assess the overall morphology of wheat starch, light microscopic images were captured as shown in Figure 1. The starch granules displayed prominent fissures, which were particularly noticeable in Pw1 granules, likely due to the isolation method, as noted by Zhang *et al.* (2019). Another notable observation was the presence of concentric layers, which were more pronounced in Pw1 starch granules, indicating a higher degree of intermolecular organization and a greater proportion of crystalline regions in this starch type. These findings were corroborated by examining the birefringence properties of the starch particles under PLM. Under polarized light, all starch particles showed the characteristic 'Maltese cross', with the crosses centered in the granules (Figure 1). No significant differences were observed in the shape or intensity of these patterns across the three types of starches.

The birefringence phenomenon is typically observed in starch particles because of the well-organized network of starch molecules in crystalline zones, compared with the disordered structure in amorphous regions (Zhang *et al.*, 2013a). CLSM was used to study the inner cavities (hilum) of starch particles. After staining with FITC, strong fluorescence was observed in the large central areas of some Pw1 and Hw3 granules (Figure 1) whereas Sw2 granules showed fluorescence primarily in the equatorial regions. This observation was aligned with prior research findings by Glaring *et al.* (2006). The effectiveness of FITC staining is linked to amylose content, as FITC binds to reducing glucose residues in starch, with higher amylose content resulting in a more pronounced staining effect (Schirmer *et al.*, 2013). A slight difference in fluorescence intensity among the three starch varieties was noted, likely due to variations in amylose content. These differences in granule morphology may result from variations in biological origin, amylose-to-amylopectin ratio, molecular structure, soil composition, climate, and genotype among different wheat varieties (Abegunde *et al.*, 2013; Huang *et al.*, 2022).

Particle size distribution

The particle size distribution data and curves of wheat starches are presented in Table 2 and Figure 2A, respectively. Starches from the three types of wheat varieties exhibited a typical unimodal distribution consisting of a broad peak of 7–56 μm. However, the distribution curve of Hw3 was found to be slightly wider, with the peak shifted to the left, indicating the presence of smaller starch particles. Xu *et al.* (2024) also reported unimodal size distribution of wheat starch, which was consistent with our findings. Furthermore, as depicted in Table 2, the D10 and D50 values of Hw3 were smaller than those of Pw1 and Sw2, suggesting the presence of a larger number of small particles in the Hw3 starch sample. The mean granule diameter (volume-weighted mean diameter or De Brouckere mean diameter, D 4,3) was 24.31, 23.88 and 22.64 μm for *PW1, Sw2 and Hw3 st*arches, respectively (Table 2). These values were slightly more significant than those obtained by Kim and Huber (2010), which were attributed to various factors, such as variations in genetic makeup, biological roots, and physiology and biochemistry of the wheat varieties (Shevkani *et al.*, 2017).

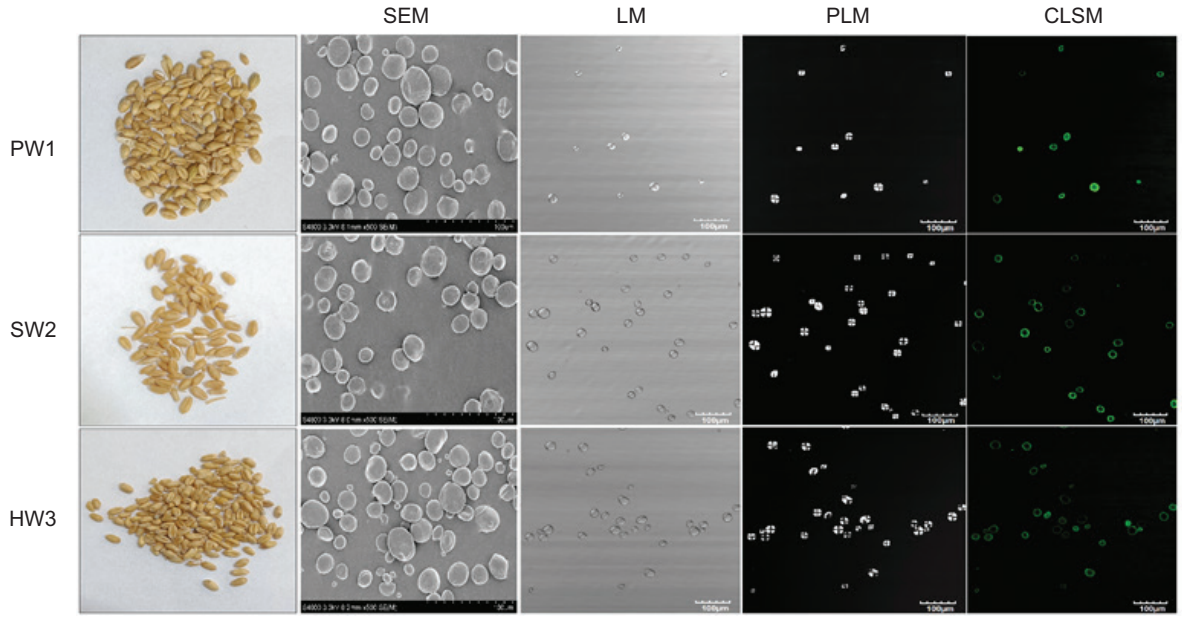

Figure 1. Confocal laser scanning micrographs (CLSM), scanning electron microscopy (SEM), polarized light micrographs (PLM), and light microscope (LM) micrographs of wheat starch.

Structural properties of wheat starch

Amylopectin chain length distribution

Amylopectin branch chain length distribution, including the average chain length in wheat starches, is displayed in Figures 2(B–D). The chain length distribution can be divided into A chains (degree of polymerization [DP] 6–12), B1 chains (DP 13–24), B2 chains (DP 25–36), and B3+ chains (DP ≥ 37) based on DP. (Hanashiro *et al.*, 1996). Pw1 and Sw2 exhibited peak maxima at DP 11 while Hw3 showed peak maxima at DP 12. The average DP for Pw1, Sw2, and Hw3 was 21.17%, 21.03%, and 20.91%, respectively, which were within the range of 21–23% reported for wheat starches in a previous study (Ao and Jane 2007). Among the wheat starches, Hw3 showed the highest proportions of B1 and A chains (45.06% and 27.79%, respectively), while Pw1 demonstrated the greater proportion of B3+ chain (12.05%), and Sw2 had the highest percentage of B2 chains (16.06%). Zhang *et al.* (2023) found that the significant proportion of longer amylopectin chains (B3+ chains) was due to an uneven distribution of macromolecules within the starch granules as well as the presence of well-organized molecules on the outer surface (Zhang *et al.*, 2023). The chain length distribution results for starches in this research were inconsistent with previous research findings (Ao and Jane 2007; Blazek *et al.*, 2009; Singh *et al.*, 2010). These differences in the chain length distribution of amylopectin in starch samples could be due to variations in the gene expression of starch synthase, environmental factors, and soil temperature.

Average molecular weight

The molecular weight distribution data for Pw1, Sw2, and Hw3 starches, such as number average molecular weight (Mn), molecular weight distribution (Mw/Mn), average molecular weight (Mw), and z-average radius of gyration (Rz) are shown in Table 2. Pw1 showed the highest Mw value (64347.64 kDa) than those of SW2 (55869.45 kDa) and HW3 (49992.05 kDa). Moreover, the *z*-average root mean square radiuses (Rz) in three starches were 221.56 nm, 257.57 nm, and 218.78 nm for Pw1, Sw2, and Hw3, respectively. These results for Mw and Rz were significantly lower than the reported values in the literature (Yoo and Jane 2002). It appeared from the results that the Mw of starch amylopectin decreased with increase in the amylose content of the samples. The higher molecular weight indicated that a highly polymerized form of amylopectin makes up the starch (Zeng *et al.*, 2016). The molecular weight distribution (Mw/Mn) reflects the degree of polydispersity in starch samples. The Mw/Mn for all starch samples varied from 2.72 to 8.35, indicating that their distinct molecular compositions contribute to the observed differences in polydispersity. Notably, the Mw/Mn value of Hw3 was lower, compared to Pw1 and Sw2, suggesting a more homogeneous amylopectin composition in Hw3 relative to other starches. Differences in the Mw/Mn values of starches are primarily driven by the amylose-to-amylopectin ratio, which directly affects the molecular weight distribution. These findings align with previous studies (Rolland-Sabaté *et al.*, 2012), which reported that starches with higher amylose content typically exhibit more uniform molecular

Table 2. Carbon atoms and chemical shifts in glucose rings by ^{13}C NMR, starch particle size distribution, and starch molecular weight.

Samples	Chemical shifts (ppm) of the C atom of glucose				Particle size distribution					Molecular weight distribution			
	C1	C4	C2, 3, 5	C6	D(0.1)/μm	D(0.5)/μm	D(0.9)/μm	D(3,2)/μm	D(4,3)/μm	Mn (kDa)	Mw (kDa)	Polydispersity (Mw/Mn)	Rz (nm)
PW1	102.04, 100.3, 98.6	80.7	71.3, 74.3	61.07	16.06 ±0.14^{a}	23.39±0.16^{a}	33.79±0.29^{b}	22.39±0.14^{a}	24.31±0.16^{a}	22654.39±0.19^{a}	64347.64±0.28^{a}	2.84±0.34^{b}	221.56±0.08^{b}
SW2	102.04, 100.3, 98.8	80.4	71.3, 74.2	61.07	15.72±0.28^{b}	22.97±0.06^{b}	33.27±0.59^{b}	21.97±0.08^{b}	23.88±0.08^{b}	6686.98±0.33^{c}	55869.45±0.32^{b}	8.35 ±0.46^{a}	257.57±0.07^{a}
HW3	102.4, 100.2, 98.5	81.7	71.3, 74.3	61.5	13.77±1.05^{c}	22.33±0.15^{b}	35.47±1.91^{a}	20.79±0.50^{c}	21.64±0.14^{c}	18336.79±0.35^{b}	49992.05±0.28^{c}	2.72±0.44^{b}	218.78±0.09^{c}

D(3,2): ratio of granule volume to overall surface area; D(4,3): mean granule diameter resulting from the volume distribution; D(0.1), D(0.5), and D(0.9): median particle diameter at 10, 50, and 90 quantiles (μm); Mw: weight-average molecular weight; Mn: number-average molecular weight; PDI: polydispersity index of molecular weight distribution); Rz: z-average radius of gyration. The data are presented as mean ± standard deviation from three separate measurements. Superscript letters (a, b, c, etc.) indicate statistical differences within the same column. Values with different superscripts are significantly different ($p < 0.05$) based on one-way ANOVA followed by Tukey's post hoc test.

weight distribution, resulting in lower Mw/Mn values. In our study, Hw3, which had the highest amylose content, exhibited the lowest Mw/Mn value.

Structural characterization of wheat starch

Crystalline structure

The wide-angle XRD crystallograms of all the starches exhibited identical characteristic diffraction peaks at 2θ values of 15.2° (singlet), 17–18° (doublet), and 23.1° (singlet), demonstrating the presence of A-type polymorphs in wheat starch (Figure 2E). The X-ray diffractograms revealed no discernible variations between the starches, indicating that the diffraction pattern remained consistent despite differences in amylopectin branch chains and particle sizes. These findings align with those of previous research (Salman *et al.*, 2009; Wang *et al.*, 2018). The relative crystallinity of the starches increased with particle size, measured as 28.48% for Pw1, 26.68% for Sw2, and 25.63% for Hw3, suggesting that larger particles contained a higher proportion of crystalline regions. According to Xie *et al.* (2024), starch granules with larger sizes exhibited increased crystallinity. Moreover, Shewry *et al.* (2009) noted that the longer amylopectin chains (DP > 37) form a stable crystalline structure. So, the higher relative crystallinity of Pw1, compared to those of Sw2 and Hw3, might be related to its bigger particle sizes and higher proportions of longer amylopectin chains.

Solid-state ^{13}C CP/MAS NMR analysis

The structural conformation of wheat starches was characterized through solid-state ^{13}C CP-MAS/NMR spectroscopy, with the resulting data (Figure 2F; Table 2). The chemical shifts for carbon atoms in starches were identified as C1, C4, C2,3,5, and C6, with their corresponding spectral regions being 92–105 ppm, 78–86 ppm, 65–77 ppm, and 55–64 ppm, respectively (Flores-Morales *et al.*, 2012). The C1 region served as a key indicator of starch variation, providing critical insights into the properties of starch (Tan *et al.*, 2007). According to Primo-Martin *et al.* (2007), the double helix symmetry and crystallinity of starch can be inferred from the multiplicity of C-1 position in glucose units. In an A-type crystalline structure, the C-1 resonance displays three distinct peaks at 100, 101, and 102 ppm. Conversely, the C-1 resonance in a B-type configuration displays two peaks at 100 ppm and 101 ppm, reflecting different sugar residues in amylopectin and amylose (Primo-Martin *et al.*, 2007). In this study, three varieties of wheat starches showed distinct signal peaks at 98–102 ppm within the C1 region, indicating the predominance of A-type allomorph, consistent with XRD results. Minor variations in these peaks between Pw1, Sw2, and Hw3 varieties suggest genetic differences influencing starch's molecular structure and crystallinity.

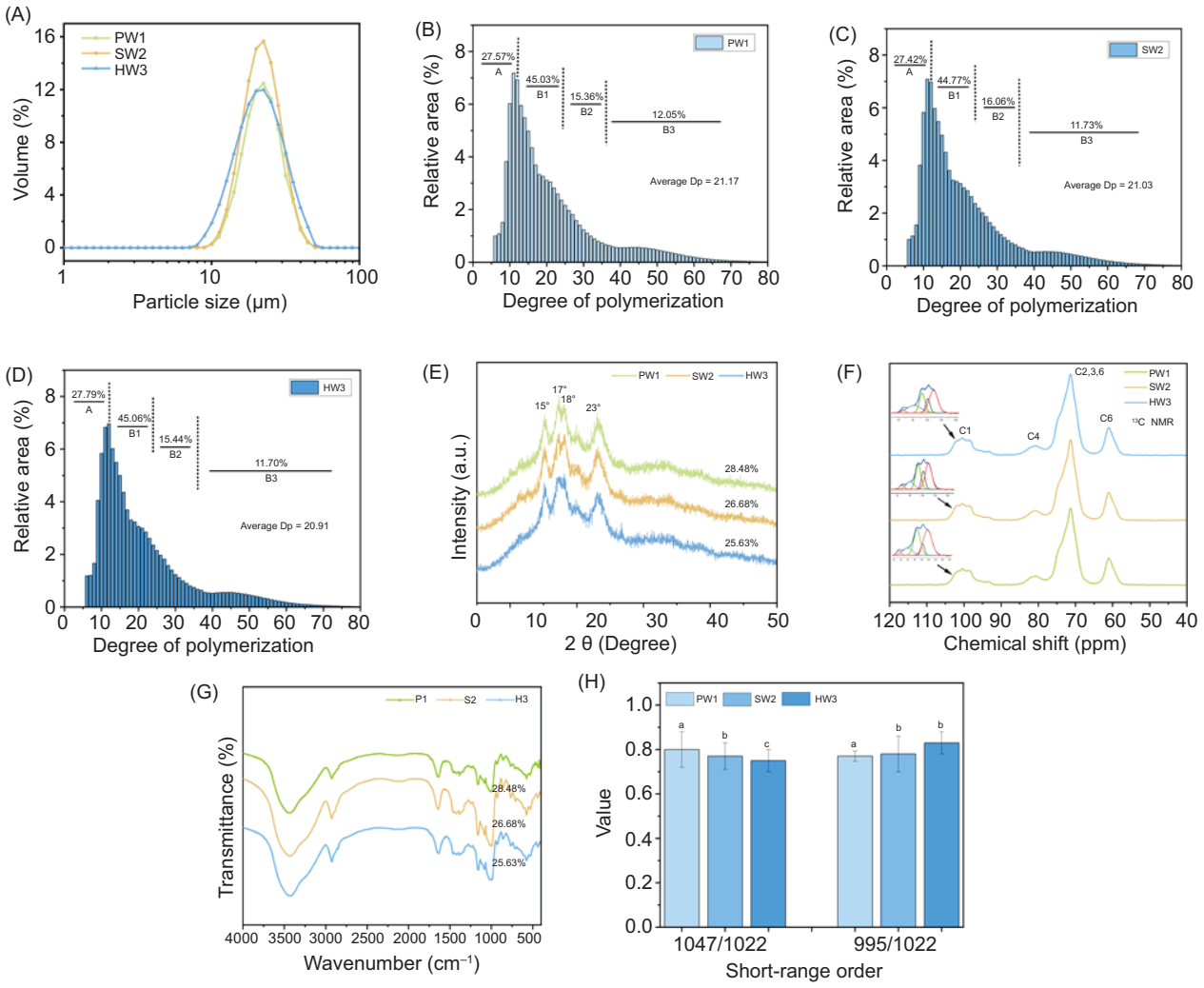

Figure 2. (A) Granules size distribution; (B–D) Chain length distribution of amylopectin of wheat starch; (E) X-ray diffraction spectrum; (F) 13C-NMR spectrum; (G) FT-IR spectra; and (H) Absorbance R1022–R995 and R1047–R1022 ratios.

Short-range order structure

The FT-IR spectra of starch samples (Figure 2G) show peaks at 2,925 cm^{-1} and 3,440 cm^{-1} for C–H deformation and O–H stretching, respectively. The 1,637 cm^{-1} absorbance corresponds to the O–H bending of water in starch amorphous zones. The anhydroglucose ring's C–O and C–C stretching is indicated by the band at 1,162 cm^{-1}, while the peaks at 1,082 and 1,015 cm^{-1} show C–O–H and C–H bending. Three C–O stretching peaks appear between 992 cm^{-1} and 1,162 cm^{-1} (Kizil *et al.*, 2002). Moreover, the crystalline region was characterized by the absorption at 1,047 cm^{-1} and 995 cm^{-1} whereas the absorption at 1,022 cm^{-1} was linked to the amorphous phase. The ratio of intensity at 995/1,022 cm^{-1} and 1,047/1,022 cm^{-1} can thus be used to characterize the degree of double helix (DD), and degree of order (DO), respectively (Liu *et al.*, 2020). Figure 2H presents the ratio values of 1,047/1,022 cm^{-1} and 995/1,022 cm^{-1} for Pw1, Sw2, and Hw3 starches. The 1,047/1,022 cm^{-1} ratio for Pw1, Sw2, and Hw3 starches were 0.8, 0.77, and 0.75, respectively. However, the 995/1,022 cm^{-1} ratio for Pw1 (0.7) was lower than those for Sw2 (0.78) and Hw3 (0.83) between three starches. Previous studies reported that higher relative crystallinity, along with an increased 1,047/1,022 cm^{-1} absorbance ratio and a reduced 995/1,022 cm^{-1} absorbance ratio, indicated a greater molecular order of double helices within starch granules (Man *et al.*, 2012; Sevenou *et al.*, 2002). In our findings, Pw1 exhibited higher crystallinity, with an increased 1,047/1,022 cm^{-1} ratio and a lower 995/1,022 cm^{-1} ratio. These results suggested that Pw1 starch had a more organized structure with increased crystalline areas compared to Sw2 and Hw3 starches, consistent with XRD analysis.

Physicochemical properties

Pasting properties of wheat starch

The pasting profile curves and corresponding characteristic parameters of wheat starch samples are shown in Figure 3A and Table 3, respectively. There was a noticeable difference in the breakdown viscosity (BD), final viscosity (FV), setback viscosity (SB), and peak viscosity (PV) of the three starches. Among the starches, Hw3 exhibited significantly higher PV and BD, compared to both Pw1 and Sw2, consistent with the results reported in a previous research (Tao *et al.*, 2016). Previous studies suggested that starches with amylopectin containing a greater proportion of DP 6–12 and a high amylose content possessed high breakdown and peak viscosities (Deng *et al.*, 2023; Noda *et al.*, 2003). Thus, the higher breakdown and peak viscosities of Hw3 were ascribed to its higher amylose content and a greater proportion of amylopectin short chains. Additionally, Hw3 showed higher final and setback viscosities, compared to those of Pw1 and Sw2. These parameters, which assess the extent of viscosity recovery as the starch paste cools, indicate associations in leached amylose chains (Ambigaipalan *et al.*, 2011). Therefore, the higher SB and FV in Hw3 starch might be explained by the quantity of amylose leached from starch particles and the presence of residual gelatinized starch. Moreover, Pw1 showed a higher pasting temperature than those of Sw2 and Hw3, which aligned with the DSC results. According to Lee *et al.* (2017), a greater amylopectin average chain length and a larger molecular weight enhanced packing efficiency, leading to a more perfect crystalline structure and, consequently, an increased pasting temperature. Therefore, the elevated pasting temperature of Pw1 could be associated with its long average chain length and increased molecular weight.

Rheological properties

Wheat starch flow behavior, as shown in Figure 3B, demonstrates that all samples are non-Newtonian fluids with shear-thinning characteristics. A Power Law equation was used to analyze the steady-shear experiment data, and Table 3 shows the produced model parameters. With high R^2 values (>0.95), the Power Law

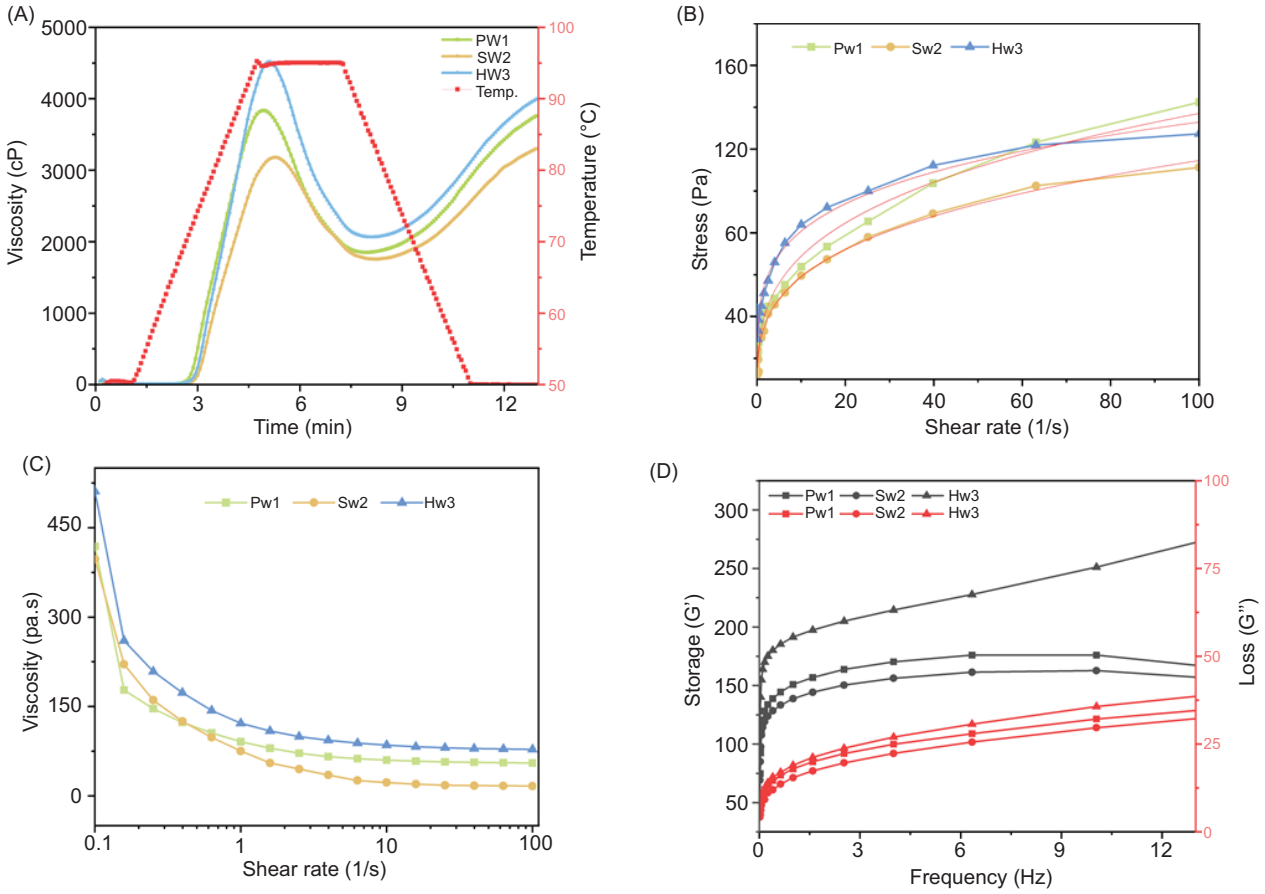

Figure 3. (A) Pasting properties; (B and C) Rheological properties, static rheological scanning; (D) dynamic rheological curve; and (E) DSC thermograms.

Table 3. Thermal, pasting, and rheological properties of wheat starch.

Sample	Thermal properties				RVA parameters					Rheological parameters ($\tau = k \cdot \gamma n$)		
	T_o (°C)	T_p (°C)	T_c (°C)	ΔH (J/g)	Pasting temperature (°C)	Peak viscosity (cP)	Breakdown (cP)	Final viscosity (cP)	Setback (cP)	K (Pa·sn)	*n*	R^2
PW1	59.68±0.26^a	62.82±0.08^a	66.43±0.03^a	9.70±0.01^a	73.16±0.43^a	3846.33±24.09^b	1993.33±10.69^b	3754.66±41.54^b	1901.66±26.76^a	34.58±0.25^a	0.29 ± 0.02^a	0.97^a
SW2	58.11±0.04^b	61.07±0.17^b	65.17±0.24^b	9.23±0.08^b	71.46±0.44^b	3163.66±17.61^c	1407.33±21.54^c	3278.33±19.03^c	1522±17.57^b	30.39±1.03^b	0.28±0.01^b	0.98^a
HW3	57.24±0.33^c	59.80±0.34^c	64.71±0.02^c	8.83±0.21^c	70.9±0.49^c	4501.66±35.90^a	2451±30.04^a	3984.33±45.98^a	1933.66±42.02^a	49.1±0.49^c	0.21±0.03^c	0.97^a

Note: Gelatinization temperatures: T_o (onset), T_p (peak), and T_c (conclusion); ΔH: gelatinization enthalpy change; τ = power-law $k \cdot \gamma n$; n: flow behavior index; γ: shear rate (s^{-1}); τ: shear stress (Pa); R^2: coefficient of correlation; k: consistency index (Pa·s^n). Measurements are done in triplicate, and the results are shown as mean values ± standard deviation. Superscript letters (a, b, c, etc.) indicate statistical differences within the same column. Values with different superscripts are significantly different ($p < 0.05$) based on one-way ANOVA followed by Tukey's post hoc test.

equation demonstrated an excellent fit to the data. The rheological behavior coefficients (*n*) for Pw1, Sw2, and Hw3 were 0.29, 0.28, and 0.21, respectively, indicating shear-thinning behavior and pseudoplastic properties of wheat starch pastes. The lower *n* value for Hw3 suggests a greater degree of shear thinning, compared to Pw1 and Sw2. Staroszczyk *et al.* (2013) found that a greater proportion of long chains within the amylopectin structure leads to a reduced shear-thinning effect. This effect could be due to the unwinding, elongation, and eventual breaking of long chains within the starch matrix with increase in shear rate. Therefore, Pw1's greater proportion of long chains (DP ≥ 37) could explain the reduced shear-thinning behavior observed, compared to Sw2 and Hw3. Figure 3C illustrates that the starch gels displayed a downward trend in viscosity with increase in shear rate, with Sw2 exhibiting the least variation in viscosity. According to Anastasiades *et al.* (2002), differences in viscosities of pre-gelatinized starches could be attributed to the concentration of swollen starch particles. Pre-gelatinized starch suspensions primarily consist of free swollen particles, which significantly influence the thickening properties of starch gel. Our findings indicate that Hw3 starch experienced a more substantial decrease in linear viscosity, compared to Pw1 and Sw2. This variation could be attributed to the higher concentration of swollen particles in Hw3 starch, consistent with the results of RVA analysis (Table 3). Figure 3D displays the dynamic rheological analysis of wheat starches. In all three starch gels, G′ surpassed G″ and showed minimal frequency dependence, suggesting that their elastic characteristics were dominant over their viscous characteristics. Previous research showed a direct relationship between G′ and amylose content (Li and Zhu, 2018). Thus, the greater G' observed in Hw3 could be due to its increased amylose content, compared to Pw1 and Sw2.

Thermal properties of wheat starch

The resulting parameters (T_o, onset temperature; T_p, peak temperature; and T_c, final gelatinization temperature) of thermal processing are the features of three types of starches (Table 3). Among the three starches, Pw1 gelatinized at a temperature (T_o) slightly more significant than those of Sw2 and Hw3. These results differ from those reported by Wickramasinghe *et al.* (2005), likely because of variations in the origins or sources of the wheat starches utilized. Moreover, Pw1 exhibited an elevated peak temperature (T_p) and conclusion/final temperature (T_c), compared to Sw2 and Hw3, indicating greater heat stability of its crystalline structure. Du *et al.* (2014) observed that short amylopectin chains had a negative correlation with the temperature of gelatinization, while long amylopectin chains exhibit a positive correlation. In this study, the elevated T_p, T_o, and T_c values for Pw1 could be linked to its higher proportion of long amylopectin chains (DP ≥ 37). The gelatinization enthalpy (ΔH) represents the degree

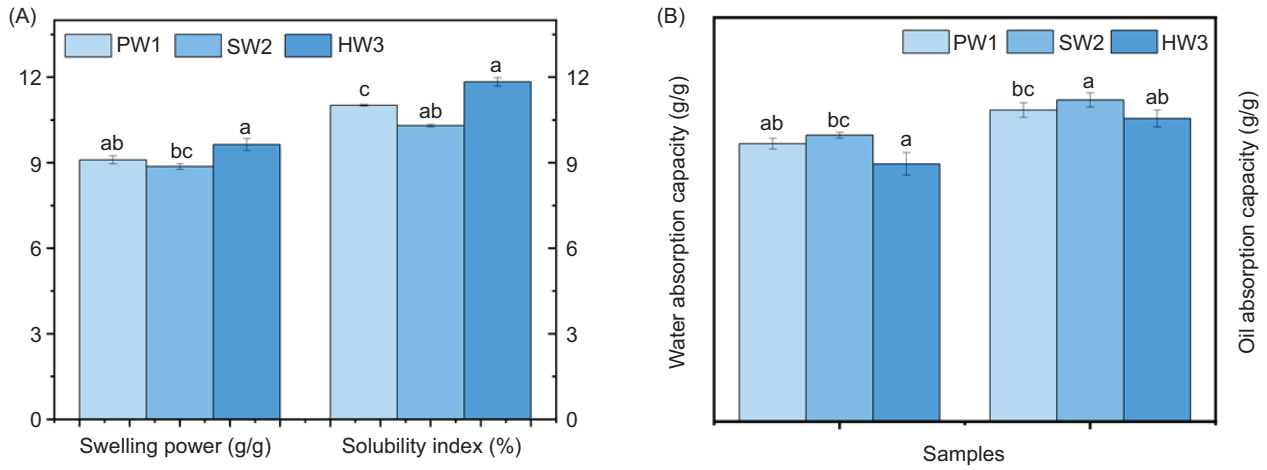

Figure 4. (A) Swelling power and water solubility; (B) Oil and water absorption capacity of wheat starch.

of crystallinity, encompassing the disruption of double helices and crystal packing. A higher ΔH value signifies a more ordered and stable starch structure (Li *et al.*, 2016b). In our analysis, Pw1 exhibited a higher ΔH of 9.7 J/g, compared to 9.2 J/g for Sw2 and 8.8 J/g for Hw3. This indicates that Pw1 starch has a more organized crystalline structure, aligning with prior observations on short-range order and crystallinity. The ΔH value observed in this study was substantially greater than those documented in previous studies (Li *et al.*, 2016a; Rosicka-Kaczmarek *et al.*, 2016), which could likely be attributed to differences in cultivation conditions.

Swelling power and water solubility

The swelling power and water solubility of wheat starches are illustrated in Figure 4A. The swelling power of Pw1, Sw2, and Hw3 were 9.1 g/g, 8.86 g/g, and 9.63 g/g, respectively. These findings were significantly below those documented by Singh *et al.* (2010). The water solubility of Pw1, Sw2, and Hw3 was 11.01%, 10.3%, and 11.83%, respectively. Among the starches, Hw3 exhibited the highest swelling power and water solubility in comparison to Pw1 and Sw2. The observed differences between three starches indicated that swelling capacity and water solubility were markedly affected by amylose concentration and distribution of amylopectin chain length in wheat starches. Li and Zhu (2017) observed that swelling power is closely linked to specific structural parameters of amylopectin, particularly short chains that enhance swelling. Similarly, Singh *et al.* (2006) identified a direct relationship between amylose content and the water solubility index, as amylose is the primary soluble component in supernatant during starch swelling, resulting in an elevated water solubility index (Singh *et al.*, 2006). Therefore, the higher swelling power and solubility index of Hw3 could be linked to its increased amylose content and greater proportion of amylopectin short chains (DP 6–12).

Water and oil absorption capacity

The water absorption capacity (WAC) and oil absorption capacity (OAC) of the three starches are illustrated in Figure 4B. Among the wheat starches, Sw2 exhibited the highest WAC at 1.70 g/g, surpassing Pw1 at 1.65 g/g and Hw3 at 1.53 g/g. In terms of OAC, the values for the wheat starch samples were 1.85 g/g for Pw1, 1.91 g/g for Sw2, and 1.80 g/g for Hw3. Sw2 starch showed higher OAC and WAC than those of Pw1 and Hw3. These results indicated that Sw2 possessed the most efficient capacity for binding water and lipids, highlighting its higher absorptive properties. Li *et al.* (2022) observed that amylose content and amylase-to-amylopectin ratio were negatively correlated with OAC and WAC, respectively. Additionally, prior studies indicated that reduced WAC and OAC are associated with a decrease in amorphous regions and an increase in crystallinity, which, in turn, limits the availability of binding sites within starch granules. Sw2, with intermediate crystallinity among the three samples, demonstrated superior binding capacity, likely because of its expanded molecular conformation, as reflected by its higher Rz. The elevated Rz suggested a greater exposure of hydroxyl groups, thereby enhancing interactions with water molecules through hydrogen bonding. These findings are consistent with those of previous studies (Chen *et al.*, 2020; Mishra and Rai 2006; Takagi *et al.*, 2017), which highlight the importance of amorphous regions, and polymorphic forms in governing water and oil adsorption. Thus, variations in WAC and OAC across the starch samples can be attributed to differences in their amylose content as well as the fine structure of starch.

Conclusions

The results of this study highlight the critical role of starch's fine structure in determining the physicochemical

characteristics of wheat starch cultivated in Pakistan. The average granule sizes for Pw1, Sw2, and Hw3 were 24 μm, 23 μm, and 21 μm, respectively, with Hw3 exhibiting the highest amylose content. Morphologically, all starches contained both A-type large, irregularly disk-like granules and B-type small, oval granules. Among the starches, Pw1 demonstrated the highest molecular weight, average degree of polymerization, R1047–R1022 ratio, relative crystallinity, and the most ordered structure. DSC analyses indicated that Pw1 had higher gelatinization temperatures compared to those of Sw2 and Hw3, which was due to its higher proportion of amylopectin long chains. The elevated pasting viscosities observed in Hw3 were associated with its large proportion of short amylopectin chains. Additionally, Hw3 exhibited significantly higher swelling power and solubility index, resulting from its higher amylose content. The Power Law equation effectively modeled the steady-shear rheological properties, with all three starches exhibiting shear-thinning behavior. Notably, Hw3 had the highest storage modulus during frequency sweep tests. Among the varieties, Sw2 showed the highest WAC and OAC, primarily because of its low amylose content. These findings offer significant insights into the diverse applications of wheat starches in the food industry.

Acknowledgment

The authors extend their appreciation to the Deanship of Scientific Research, Vice Presidency for Graduate Studies and Scientific Research, King Faisal University, Saudi Arabia, for funding this study. This work was funded by the National Natural Science Foundation of China (No. 32272351).

Authors Contributions

Saddam Mustafa: data curation, methodology, and writing – original draft preparation. Haiam O. Elkatry and Abdelrahman R. Ahmed: validation and formal analysis. Chengyi Sun and Zhijie Zhu: resources, project administration, and investigation. Mohamed El Oirdi and Hossam S. El-Beltagi: visualization, writing – review, and editing. Xianfeng Du: conceptualization and supervision.

Conflict of Interest

The authors declared no competing financial interest.

Funding

This work was supported by the Deanship of Scientific Research, Vice Presidency for Graduate Studies and Scientific Research, King Faisal University, Saudi Arabia (Grant No.: KFU242229).

References

Abegunde O.K., Mu T.H., Chen J.W. and Deng F.M., 2013. Physicochemical characterization of sweet potato starches popularly used in Chinese starch industry. Food Hydrocoll. 33(2):169–177. https://doi.org/10.1016/j.foodhyd.2013.03.005

Ambigaipalan P., Hoover R., Donner E., Liu Q., Jaiswal S., Chibbar R., Nantanga K. and Seetharaman K., 2011. Structure of faba bean, black bean and pinto bean starches at different levels of granule organization and their physicochemical properties. Food Res Int. 44(9):2962–2974. https://doi.org/10.1016/j.foodres.2011.07.006

Anastasiades A., Thanou S., Loulis D., Stapatoris A. and Karapantsios T., 2002. Rheological and physical characterization of pregelatinized maize starches. J Food Eng. 52(1):57–66. https://doi.org/10.1016/S0260-8774(01)00086-3

Ao Z. and Jane J.l., 2007. Characterization and modeling of the A- and B-granule starches of wheat, triticale, and barley. Carbohydr Polym. 67(1):46–55. https://doi.org/10.1016/j.carbpol.2006.04.013

Bashir K., Swer T.L., Prakash K.S. and Aggarwal M., 2017. Physicochemical and functional properties of gamma irradiated whole wheat flour and starch. Food Sci Technol (LWT). 76:131–139. https://doi.org/10.1016/j.lwt.2016.10.050

Blazek J., Salman H., Rubio A.L., Gilbert E., Hanley T. and Copeland L., 2009. Structural characterization of wheat starch granules differing in amylose content and functional characteristics. Carbohydr Polym. 75(4):705–711. https://doi.org/10.1016/j.carbpol.2008.09.017

Cai L. and Shi Y.-C., 2010. Structure and digestibility of crystalline short-chain amylose from debranched waxy wheat, waxy maize, and waxy potato starches. Carbohy Polym. 79(4):1117–1123. https://doi.org/10.1016/j.carbpol.2009.10.057

Chen Y., Dai G. and Gao Q., 2020. Preparation and properties of granular cold-water-soluble porous starch. Int J Biol Macromol. 144:656–662. https://doi.org/10.1016/j.ijbiomac.2019.12.060

Debon S.J. and Tester R.F., 2000. *In vivo* and *in vitro* annealing of starches. Royal Soc Chem (Sp Pub). 251:270–276. https://doi.org/10.1533/9781845698355.4.270

Deng C., Wang B., Jin Y., Yu Y., Zhang Y., Shi S., Wang Y., Zheng M., Yu Z. and Zhou Y., 2023. Effects of starch multiscale structure on the physicochemical properties and digestibility of Radix Cynanchi bungei starch. Int J Biol Macromol. 253:126873. https://doi.org/10.1016/j.ijbiomac.2023.126873

de Souza Fernandes D., Dos Santos T.P.R., Fernandes A.M. and Leonel M., 2019. Harvest time optimization leads to the production of native cassava starches with different properties. Int J Biol Macromol. 132:710–721. https://doi.org/10.1016/j.ijbiomac.2019.03.245

Dos Santos T.P.R., Leonel M., Garcia É.L., do Carmo E.L. and Franco C.M.L., 2016. Crystallinity, thermal and pasting properties of starches from different potato cultivars grown in Brazil. Int J Biol Macromol. 82:144–149. https://doi.org/10.1016/j.ijbiomac.2015.10.091

Du, S.K., Jiang, H., Ai, Y. and Jane J.L., 2014. Physicochemical properties and digestibility of common bean (*Phaseolus vulgaris* L.) starches. Carbohydr Polym. 108:200–205. https://doi.org/10.1016/j.carbpol.2014.03.004

Flores-Morales A., Jiménez-Estrada M. and Mora-Escobedo R., 2012. Determination of the structural changes by FT-IR, Raman, and CP/MAS 13C NMR spectroscopy on retrograded starch of maize tortillas. Carbohydr. Polym. 87(1):61–68. https://doi.org/10.1016/j.carbpol.2011.07.011

Glaring M.A., Koch C.B. and Blennow A., 2006. Genotype-specific spatial distribution of starch molecules in the starch granule: a combined CLSM and SEM approach. Biomacromolecules. 7(8):2310–2320. https://doi.org/10.1021/bm060216e

Gunaratne A., Gan R., Wu K., Kong X., Collado L., Arachchi L.V., Kumara K., Pathirana S.M. and Corke H., 2018. Physicochemical properties of mung bean starches isolated from four varieties grown in Sri Lanka. Starch-Stärke. 70(3–4):1700129. https://doi.org/10.1002/star.201700129

Hanashiro I., Abe J.I. and Hizukuri S., 1996. A periodic distribution of the chain length of amylopectin as revealed by high-performance anion-exchange chromatography. Carbohydr Res. 283:151–159. https://doi.org/10.1016/0008-6215(95)00408-4

Huang J., Wang Z., Fan L. and Ma S., 2022. A review of wheat starch analyses: methods, techniques, structure and function. Int J Biol Macromol. 203:130–142. https://doi.org/10.1016/j.ijbiomac.2022.01.149

Hung P.V., Maeda T. and Morita N., 2007. Study on physicochemical characteristics of waxy and high-amylose wheat starches in comparison with normal wheat starch. Starch-Stärke. 59(3–4):125–131. https://doi.org/10.1002/star.200600577

Karwasra B.L., Gill B.S. and Kaur M., 2017. Rheological and structural properties of starches from different Indian wheat cultivars and their relationships. Int J Food Prop. 20(Sup1):S1093–S1106. https://doi.org/10.1080/10942912.2017.1328439

Kim H.S. and Huber K.C., 2010. Physicochemical properties and amylopectin fine structures of A- and B-type granules of waxy and normal soft wheat starch. J Cereal Sci. 51(3):256–264. https://doi.org/10.1016/j.jcs.2009.11.015

Kizil R., Irudayaraj J. and Seetharaman K., 2002. Characterization of irradiated starches by using FT-Raman and FTIR spectroscopy. J Agric Food Chem. 50(14):3912–3918. https://doi.org/10.1021/jf011652p

Kumar R. and Khatkar B., 2017. Thermal, pasting and morphological properties of starch granules of wheat (*Triticum aestivum* L.) varieties. J Food Sci Technol. 54:2403–2410. https://doi.org/10.1007/s13197-017-2681-x

Labuschagne M.T., Geleta N. and Osthoff G., 2007. The influence of environment on starch content and amylose to amylopectin ratio in wheat. Starch-Stärke. 59(5):234–238. https://doi.org/10.1002/star.200600542

Lee S., Lee J.H. and Chung H.J., 2017. Impact of diverse cultivars on molecular and crystalline structures of rice starch for food processing. Carbohydr Polym. 169:33–40. https://doi.org/10.1016/j.carbpol.2017.03.091

Li W., Gao J., Wu G., Zheng J., Ouyang S., Luo Q. and Zhang G., 2016a. Physicochemical and structural properties of A- and B-starch isolated from normal and waxy wheat: effects of lipids removal. Food Hydrocol. 60:364–373. https://doi.org/10.1016/j.foodhyd.2016.04.011

Li Z., Kong X., Zhou X., Zhong K., Zhou S. and Liu X., 2016b. Characterization of multi-scale structure and thermal properties of Indica rice starch with different amylose contents. RSC Adv. 6(109):107491–107497. https://doi.org/10.1039/C6RA17922C

Li N., Niu M., Zhang B., Zhao S., Xiong S. and Xie F., 2017. Effects of concurrent ball milling and octenyl succinylation on structure and physicochemical properties of starch. Carbohydr Polym. 155:109–116. https://doi.org/10.1016/j.carbpol.2016.08.063

Li B., Wang Y., Zhu L., Huang C., Zhang Y., Zhao Y., Wu G. and Tan L., 2022. Starch characterizations of two kinds of seedless Artocarpus altilis (Parkinson) Fosberg originated from China. Food Hydrocol. 123:107145. https://doi.org/10.1016/j.foodhyd.2021.107145

Li W., Xiao X., Zhang W., Zheng J., Luo Q., Ouyang S. and Zhang G., 2014. Compositional, morphological, structural and physicochemical properties of starches from seven naked barley cultivars grown in China. Food Res Int. 58:7–14. https://doi.org/10.1016/j.foodres.2014.01.053

Li S., Zhou Y., Liu M., Zhang Y. and Cao S., 2015. Nutrient composition and starch characteristics of Quercus glandulifera Bl. seeds from China. Food Chem. 185:371–376. https://doi.org/10.1016/j.foodchem.2015.03.147

Li G. and Zhu F., 2017. Amylopectin molecular structure in relation to physicochemical properties of quinoa starch. Carbohydr Polym. 164:396–402. https://doi.org/10.1016/j.carbpol.2017.02.014

Li G. and Zhu F., 2018. Rheological properties in relation to molecular structure of quinoa starch. Int J Biol Macromol. 114:767–775. https://doi.org/10.1016/j.ijbiomac.2018.03.039

Li G.H., Ye B.B., Wu J.D., Hou Z.Y., Chu Z. S., Zheng B.H. and Yang Y.Z., 2020. Changing characteristics on contents and forms of nitrogen and phosphorus in sediment during *in-situ* physical elution. Res Environ Sci. 33(2):392–401. https://doi.org/10.13198/j.issn.1001-6929.2019.06.04

Liu C., Liu L., Li L., Hao C., Zheng X., Bian K., Zhang J. and Wang X., 2015. Effects of different milling processes on whole wheat flour quality and performance in steamed bread making. Food Sci Technol (LWT). 62(1):310–318. https://doi.org/10.1016/j.lwt.2014.08.030

Liu D., Tang W., Xin Y., Yang J., Yuan L., Huang X., Yin J., Nie S. and Xie M., 2020. Comparison on structure and physicochemical properties of starches from Adzuki bean and Dolichos beans. Food Hydrocol. 105:105784. https://doi.org/10.1016/j.foodhyd.2020.105784

Man J., Yang Y., Zhang C., Zhou X., Dong Y., Zhang F., Liu Q. and Wei C., 2012. Structural changes of high-amylose rice starch residues following *in vitro* and *in vivo* digestion. J Agric Food Chem. 60(36):9332–9341. https://doi.org/10.1021/jf302966f

Maningat C.C., Seib P.A., Bassi S.D., Woo K.S. and Lasater G.D., 2009. Wheat starch: production, properties, modification and uses. In: Miller J. and Whistler, J. (Eds.) Starch. Chemistry and Technology. Elsevier, Amsterdam, the Netherlands, pp. 441–510. https://doi.org/10.1016/S1082-0132(08)X0009-3

Mishra S. and Rai T., 2006. Morphology and functional properties of corn, potato and tapioca starches. Food Hydrocol. 20(5):557–566. https://doi.org/10.1016/j.foodhyd.2005.01.001

Mitura K., Cacak-Pietrzak G., Feledyn-Szewczyk B., Szablewski T. and Studnicki M., 2023. Yield and grain quality of common wheat (*Triticum aestivum* L.) depending on the different farming systems (organic vs. integrated vs. conventional). Plants. 12(5):1022. https://doi.org/10.3390/plants12051022

Noda T., Nishiba Y., Sato T. and Suda I., 2003. Properties of starches from several low-amylose rice cultivars. Cereal Chem. 80(2):193–197. https://doi.org/10.1094/CCHEM.2003.80.2.193

Primo-Martin C., Van Nieuwenhuijzen N., Hamer R. and Van Vliet T., 2007. Crystallinity changes in wheat starch during the bread-making process: starch crystallinity in the bread crust. J Cereal Sci. 45(2):219–226. https://doi.org/10.1016/j.jcs.2006.08.009

Rolland-Sabaté A., Sánchez T., Buléon A., Colonna P., Jaillais B., Ceballos H. and Dufour D., 2012. Structural characterization of novel cassava starches with low and high-amylose contents in comparison with other commercial sources. Food Hydrocol. 27(1):161–174. https://doi.org/10.1016/j.foodhyd.2011.07.008

Rosicka-Kaczmarek J., Makowski B., Nebesny E., Tkaczyk M., Komisarczyk A. and Nita Z., 2016. Composition and thermodynamic properties of starches from facultative wheat varieties. Food Hydrocol. 54:66–76. https://doi.org/10.1016/j.foodhyd.2015.09.014

Salman H., Blazek J., Lopez-Rubio A., Gilbert E.P., Hanley T. and Copeland L., 2009. Structure–function relationships in A- and B-granules from wheat starches of similar amylose content. Carbohydr Polym. 75(3):420–427. https://doi.org/10.1016/j.carbpol.2008.08.001

Schirmer M., Höchstötter A., Jekle M., Arendt E. and Becker T., 2013. Physicochemical and morphological characterization of different starches with variable amylose/amylopectin ratio. Food Hydrocol. 32(1):52–63. https://doi.org/10.1016/j.foodhyd.2012.11.032

Seib P.A., Steele J.L. and Chung O.K., 1997. Wheat starch as a quality determinant. In: Proceedings, International Wheat Quality Conference, *May 18–22,* Manhattan, KS. Grain Marketing and Production Research Center, Manhattan, KS, pp. 61–82.

Sevenou O., Hill S., Farhat I. and Mitchell J., 2002. Organisation of the external region of the starch granule as determined by infrared spectroscopy. Int J Biol Macromol. 31(1–3):79–85. https://doi.org/10.1016/S0141-8130(02)00067-3

Shevkani K., Singh N., Bajaj R. and Kaur A., 2017. Wheat starch production, structure, functionality and applications—a review. Int J Food Sci Technol. 52(1):38–58. https://doi.org/10.1111/ijfs.13266

Shevkani K., Singh N., Singh S., Ahlawat A.K. and Singh A.M., 2011. Relationship between physicochemical and rheological properties of starches from Indian wheat lines. Int J Food Sci Technol. 46(12):2584–2590. https://doi.org/10.1111/j.1365-2621.2011.02787.x

Shewry P.R., Underwood C., Wan Y., Lovegrove A., Bhandari D., Toole G., Mills E.C., Denyer K. and Mitchell R.A., 2009. Storage product synthesis and accumulation in developing grains of wheat. J Cereal Sci. 50(1):106–112. https://doi.org/10.1016/j.jcs.2009.03.009

Singh N., Kaur M., Sandhu K.S. and Guraya H.S., 2004. Physicochemical, thermal, morphological and pasting properties of starches from some Indian black gram (*Phaseolus mungo* L.) cultivars. Starch-Stärke. 56(11):535–544. https://doi.org/10.1002/star.200400290

Singh J., McCarthy O.J. and Singh H., 2006. Physico-chemical and morphological characteristics of New Zealand Taewa (Maori potato) starches. Carbohydr Polym. 64(4):569–581. https://doi.org/10.1016/j.carbpol.2005.11.013

Singh S., Singh N., Isono N. and Noda T., 2010. Relationship of granule size distribution and amylopectin structure with pasting, thermal, and retrogradation properties in wheat starch. J Agric Food Chem. 58(2):1180–1188. https://doi.org/10.1021/jf902753f

Song Z., Zhong Y., Tian W., Zhang C., Hansen A.R., Blennow A., Liang W. and Guo D., 2020. Structural and functional characterizations of α-amylase-treated porous popcorn starch. Food Hydrocol. 108:105606. https://doi.org/10.1016/j.foodhyd.2019.105606

Staroszczyk H., Fiedorowicz M., Opalińska-Piskorz J. and Tylingo R., 2013. Rheology of potato starch chemically modified with microwave-assisted reactions. Food Sci Technol (LWT). 53(1):249–254. https://doi.org/10.1016/j.lwt.2013.01.009

Takagi H., Suzuki S., Akdogan G. and Kitamura S., 2017. Surface structure and water adsorption behavior of waxy/amylose extender (wx/ae) double-mutant rice starch. Starch-Stärke. 69(11–12):1600374. https://doi.org/10.1002/star.201600374

Tan I., Flanagan B.M., Halley P.J., Whittaker A.K. and Gidley M.J., 2007. A method for estimating the nature and relative proportions of amorphous, single, and double-helical components in starch granules by 13C CP/MAS NMR. Biomacromolecules. 8(3):885–891. https://doi.org/10.1021/bm060988a

Tao H., Wang P., Wu F., Jin Z. and Xu X., 2016. Particle size distribution of wheat starch granules in relation to baking properties of frozen dough. Carbohydr Polym. 137:147–153. https://doi.org/10.1016/j.carbpol.2015.10.063

Tester R.F. and Karkalas J., 2001. The effects of environmental conditions on the structural features and physico-chemical properties of starches. Starch-Stärke. 53(10):513–519. https://doi.org/10.1002/1521-379X(200110)53:10<513::AID-STAR513>3.0.CO;2-5

Wang S., Luo H., Zhang J., Zhang Y., He Z. and Wang S., 2014. Alkali-induced changes in functional properties and in vitro digestibility of wheat starch: the role of surface proteins and lipids. J Agric Food Chem. 62(16):3636–3643. https://doi.org/10.1021/jf500249w

Wang S., Wang J., Zhang W., Li C., Yu J. and Wang S., 2015. Molecular order and functional properties of starches from three waxy wheat varieties grown in China. Food Chem. 181:43–50. https://doi.org/10.1016/j.foodchem.2015.02.065

Wang L., Yu X., Yang Y., Chen X., Wang Q., Zhang X., Ran L. and Xiong F., 2018. Morphology and physicochemical properties of starch in wheat superior and inferior grains. Starch-Stärke. 70(3–4):1700177. https://doi.org/10.1002/star.201700177

Wickramasinghe H.A.M., Miura H., Yamauchi H. and Noda T., 2005. Comparison of the starch properties of Japanese wheat varieties with those of popular commercial wheat classes from the USA, Canada and Australia. Food Chem. 93(1):9–15. https://doi.org/10.1016/j.foodchem.2004.08.049

Wongsagonsup R., Pujchakarn T., Jitrakbumrung S., Chaiwat W., Fuongfuchat A., Varavinit S., Dangtip S. and Suphantharika M., 2014. Effect of cross-linking on physicochemical properties of Tapioca starch and its application in soup product. Carbohydr Polym. 101:656–665. https://doi.org/10.1016/j.carbpol.2013.09.100

Xia H., Li Y. and Gao Q., 2016. Preparation and properties of RS4 citrate sweet potato starch by heat-moisture treatment. Food Hydrocol. 55:172–178. https://doi.org/10.1016/j.foodhyd.2015.11.008

Xie X., Chen J., Cheng L., Zhang B., Zhu H., Xu C. and Liang D., 2024. Physicochemical properties of different size fractions of potato starch cultivated in Highland China. Int J Biol Macromol. 256:128065. https://doi.org/10.1016/j.ijbiomac.2023.128065

Xu C., Li C., Li E. and Gilbert R.G., 2024. Insights into wheat-starch biosynthesis from two-dimensional macromolecular structure. Carbohydr Polym. 337:122190. https://doi.org/10.1016/j.carbpol.2024.122190

Yoo S.H. and Jane J.l., 2002. Structural and physical characteristics of waxy and other wheat starches. Carbohydr Polym. 49(3):297–305. https://doi.org/10.1016/S0144-8617(01)00338-1

Zeng F., Gao Q.Y., Han Z., Zeng X.A. and Yu S.J., 2016. Structural properties and digestibility of pulsed electric field treated waxy rice starch. Food Chem. 194:1313–1319. https://doi.org/10.1016/j.foodchem.2015.08.104

Zhang Y., Dai Y., Hou H., Li X., Dong H., Wang W. and Zhang H., 2020. Ultrasound-assisted preparation of octenyl succinic anhydride modified starch and its influence mechanism on the quality. Food Chem X. 5:100077. https://doi.org/10.1016/j.fochx.2020.100077

Zhang Q., Duan H., Zhou Y., Zhou S., Ge X., Shen H., Li W. and Yan W., 2023. Effect of dry heat treatment on multi-structure, physicochemical properties, and *in vitro* digestibility of potato starch with controlled surface-removed levels. Food Hydrocol. 134:108062. https://doi.org/10.1016/j.foodhyd.2022.108062

Zhang B., Li X., Liu J., Xie F. and Chen L., 2013a. Supramolecular structure of A- and B-type granules of wheat starch. Food Hydrocol. 31(1):68–73. https://doi.org/10.1016/j.foodhyd.2012.10.006

Zhang Z., Tian X., Wang P., Jiang H. and Li W., 2019. Compositional, morphological, and physicochemical properties of starches from red Adzuki bean, chickpea, Faba bean, and Baiyue bean grown in China. Food Sci Nutr. 7(8):2485–2494. https://doi.org/10.1002/fsn3.865

Zhang H., Zhang W., Xu C. and Zhou X., 2013b. Morphological features and physicochemical properties of waxy wheat starch. Int J Biol Macromol. 62:304–309. https://doi.org/10.1016/j.ijbiomac.2013.09.030

Zhao T., Li X., Zhu R., Ma Z., Liu L., Wang X. and Hu X., 2019. Effect of natural fermentation on the structure and physicochemical properties of wheat starch. Carbohydr Polym. 218:163–169. https://doi.org/10.1016/j.carbpol.2019.04.061

Zhou Y., Zhao D., Winkworth-Smith C.G., Foster T.J., Nirasawa S., Tatsumi E. and Cheng Y., 2015. Effect of a small amount of sodium carbonate on Konjac glucomannan-induced changes in wheat starch gel. Carbohydr Polym. 116:182–188. https://doi.org/10.1016/j.carbpol.2014.02.087